

Structure of the Fermi hole at surfaces

Manoj K. Harbola and Virahat Sahni

*Department of Physics, Brooklyn College of the City University of New York, Brooklyn, New York 11210
and The Graduate School and University Center of the City University of New York, 33 West 42nd Street,
New York, New York 10036*

(Received 15 January 1987)

We have extended the work of Sahni and Bohnen to more emphatically demonstrate that as an electron is removed from within a metal to infinity outside, its average exchange charge density is not localized to the surface region but rather spreads throughout the entire semi-infinite crystal. Thus, asymptotically, the Fermi hole does not constitute part of the image charge at the surface. In addition to the planar-averaged density, we have also studied the structure of the charge in planes parallel to the surface as well as in the plane perpendicular to the surface encompassing the axis of electron removal. Comparison of the quantum-mechanical and classical charge distributions in the planes parallel to the surface show the two to differ significantly. We also prove analytically that independent of the electron position in the vacuum (positive half-space) region, there is always charge at minus infinity in the metal.

I. INTRODUCTION AND DEFINITIONS

It had long been believed that the image charge of an electron at a metal surface is the exchange and correlation hole that it leaves behind at the surface.¹⁻⁵ (The exchange hole, also known as the Fermi hole, is a consequence of the Pauli exclusion principle which prohibits two electrons of parallel spin being in the same state. The correlation hole arises due to the classical Coulomb repulsion between the electrons.) However, in their analysis of the *average* exchange charge density, Sahni and Bohnen^{6,7} discovered that as an electron is pulled out of a metal, its Fermi hole instead of being localized to the surface region starts spreading into the interior of the crystal. The width of the hole depends upon the position of the electron and keeps increasing as the electron is pulled further and further out. Thus, in the asymptotic limit, when the electron is very far from the surface, Sahni and Bohnen concluded that its Fermi hole would extend throughout the crystal. Exchange effects, which are a consequence of the statistics of the particles involved, thus do not contribute to the structure of the image charge at a metal surface. In this asymptotic region the image charge is due strictly to Coulomb correlation.

In arriving at their conclusions, Sahni and Bohnen studied only the behavior of the charge density averaged over the planes parallel to the surface. Their analysis therefore did not include the details of the structure of the average exchange charge distribution in these planes. Furthermore, their study extended up to electron positions of a maximum of approximately two Fermi wavelengths from the surface for typical metallic density profiles. In our paper we more emphatically demonstrate the spreading of the Fermi hole through the volume of the crystal by considering electron positions up to approximately ten Fermi wavelengths from the surface. In addition, we study the structure of the aver-

age exchange charge in the plane perpendicular to the surface encompassing the axis of electron removal. Since we know that the classical image charge gives rise to an image potential, we also make comparisons between the classical and quantum-mechanical charge distribution in the planes parallel to the surface. Finally, by deriving an analytical expression for the exchange charge density deep in the bulk, we show that irrespective of the electron position the exchange charge extends all the way up to minus infinity (with the vacuum existing in the positive half-space). Thus while reaffirming the conclusions of Sahni and Bohnen, we provide in this work significant new insights into the structure of the Fermi hole at a metal surface.

The average exchange charge density $\rho_x(\mathbf{r}, \mathbf{r}')$ at \mathbf{r}' due to an electron of momentum \mathbf{k} at \mathbf{r} is defined⁸ in terms of the electronic wave functions $\Psi_{\mathbf{k}}(\mathbf{r})$ as⁹

$$\rho_x(\mathbf{r}, \mathbf{r}') = \frac{\sum_{\mathbf{k}} \sum_{\mathbf{k}'} \Psi_{\mathbf{k}}^*(\mathbf{r}) \Psi_{\mathbf{k}'}^*(\mathbf{r}') \Psi_{\mathbf{k}}(\mathbf{r}) \Psi_{\mathbf{k}'}(\mathbf{r}')}{\sum_{\mathbf{k}} \Psi_{\mathbf{k}}^*(\mathbf{r}) \Psi_{\mathbf{k}}(\mathbf{r})} . \quad (1)$$

The wave functions $\Psi_{\mathbf{k}}(\mathbf{r})$, in the jellium model approximation of a metal surface, have the general form

$$\Psi_{\mathbf{k}}(\mathbf{r}) = - \left[\frac{2}{V} \right]^{1/2} \phi_k(x) e^{i\mathbf{k}_{\parallel} \cdot \mathbf{x}_{\parallel}} , \quad (2)$$

where $\phi_k(x)$ is the part of the wave function in the direction perpendicular to the surface with k and x being the components of the momentum and position vectors in that direction, and \mathbf{k}_{\parallel} and \mathbf{x}_{\parallel} are the corresponding components in the plane of the surface. Due to the depletion of charge about each electron, the average exchange charge density satisfies the charge conservation sum rule:

$$\int \rho_x(\mathbf{r}, \mathbf{r}') d\mathbf{r}' = 1 . \quad (3)$$

In terms of the dimensionless variable $y = k_F x$, $y' = k_F x'$, $\mathbf{y}_\parallel = k_F \mathbf{x}_\parallel$, $\mathbf{y}'_\parallel = k_F \mathbf{x}'_\parallel$, $q = k/k_F$, and $q' = k'/k_F$, where k_F is the Fermi momentum, the average exchange charge density at $(y', \mathbf{y}'_\parallel)$ due to an electron at y is given by the expression (see Appendix A)

$$\frac{\rho_x(y, y'; \mathbf{y}'_\parallel)}{\bar{\rho}/2} = \frac{36}{\rho_n(y)} \left| \int_0^1 dq \phi_q^*(y) \phi_q(y') \frac{(1-q^2)^{1/2}}{|\mathbf{y}'_\parallel|} \times J_1((1-q^2)^{1/2} |\mathbf{y}'_\parallel|) \right|^2, \quad (4)$$

where $J_1(x)$ is the first-order Bessel function, and $\rho_n(y)$ is the electronic density normalized with respect to the bulk value $\bar{\rho} = k_F^3/3\pi^2$;

$$\rho_n(y) = \frac{\rho(y)}{\bar{\rho}} = 3 \int_0^1 dq (1-q^2) |\phi_q(y)|^2. \quad (5)$$

It is from Eq. (4) that one can study the behavior of the charge distribution in planes parallel to the surface

$$\frac{\rho_x(y, y')}{3k_F/\pi} = \frac{4}{\rho_n(y)} \int_0^\infty \frac{d|\mathbf{y}'_\parallel|}{|\mathbf{y}'_\parallel|} \left| \int_0^1 dq \phi_q^*(y) \phi_q(y') (1-q^2)^{1/2} J_1(\sqrt{1-q^2} |\mathbf{y}'_\parallel|) \right|^2. \quad (8)$$

The planar-averaged density may also be written as⁷

$$\frac{\rho_x(y, y')}{3k_F/\pi} = \frac{F(y, y')}{\rho_n(y)}, \quad (9)$$

where

$$F(y, y') = 2 \int_0^1 dq (1-q^2) \times \int_0^q dq' [\phi_{qq'}(y', y) + \phi_{qq'}(y, y')], \quad (10)$$

and where

$$\phi_{qq'}(y, y') = \phi_q^*(y) \phi_{q'}^*(y') \phi_q(y') \phi_{q'}(y). \quad (11)$$

It is evident that for computational purposes Eq. (9) is more useful as both the integrals are momentum space integrals ranging from zero to one, whereas in Eq. (8) one of the integrals is a spatial integral ranging from zero to infinity. However, the two different expressions for the planar-averaged density serve as a check on the numerical results obtained. The analytical equivalence of these expressions is shown in Appendix A.

II. RESULTS

We perform our initial set of calculations for the step-potential model¹⁰⁻¹² of a surface. We do so for the following reasons. First, the model describes quite well the qualitative aspects of the metal-vacuum interface. As opposed to the infinite barrier model,¹⁰⁻¹² where the electronic density is forced to vanish at the barrier, the step model permits the electronic density to decay exponentially into the vacuum region as it must. Secondly, because one is dealing with exponential functions in the classically forbidden region, it is possible to consider

spreading radially from the axis along which the electron is being removed. On substituting $\mathbf{y}'_\parallel = \mathbf{0}$ in Eq. (4) we obtain the expression for the exchange charge density in the plane perpendicular to the surface and encompassing the axis of electron removal:

$$\frac{\rho_x(\mathbf{r}, \mathbf{r}')}{\bar{\rho}/2} \Big|_{\mathbf{x}_\parallel = \mathbf{x}'_\parallel = 0} = \frac{9}{\rho_n(y)} \left| \int_0^1 dq (1-q^2) \phi_q^*(y) \phi_q(y') \right|^2. \quad (6)$$

The final quantity we need in our study is the planar-averaged exchange charge density $\rho_x(y, y')$ which is the total charge in a plane at y' parallel to the surface. This is defined as

$$\rho_x(y, y') = \frac{1}{A} \int d\mathbf{x}_\parallel \int d\mathbf{x}'_\parallel \rho_x(\mathbf{r}, \mathbf{r}'), \quad (7)$$

where A is the surface area. From Eq. (4) we see that the planar-averaged charge at y' for an electron at y is

electron positions far from the metal surface. We note, however, that the model is not a very accurate representation of the effective potential seen by electrons at the surface.^{11,12} For high-density metals it too strongly reflects the electrons back into the metal, whereas for low-density metals, it is too weakly confining. As a consequence, the magnitude (and sign) of various properties can differ significantly from those of fully self-consistent¹³ or more accurate representations^{14,15} of the effective potential at the surface. However, for the qualitative feature of the Fermi hole that we wish to describe, it is more than adequate.

For the step model, for which the effective potential at the surface is $V_{\text{eff}} = W\Theta(x)$, the electronic wave functions in the direction of the inhomogeneity are^{10,11}

$$\phi_k(x) = \sin[kx + \delta(k)]\Theta(-x) - \frac{k}{p} \exp[-(p^2 - k^2)^{1/2}x]\Theta(x), \quad (12)$$

where the phase shifts are given by $\delta(k) = \sin^{-1}(k/p)$ and where $p^2 = 2W$. In this model all the surface properties including the average exchange charge density can be written in terms of universal functions of the barrier height parameter $\beta = k_F/p$. The parameter β is related to the barrier height W by $\beta^{-2} = W/(k_F^2/2)$. For our calculations we have chosen a low barrier height $W = 1.5(k_F^2/2)$ or $\beta = 0.8165$. This choice of parameter corresponds to a typical metallic density profile at the surface.^{11,12} For this choice of barrier height, the jellium edge position¹¹ determined by charge neutrality is at $y_a = -0.2895$.

We begin our analysis by considering the cross section through the exchange hole given by Eq. (6). In the

infinite barrier model (as discussed in both Refs. 1 and 7), there is a distinct flattening of the curves as the electron is moved through the surface. This, of course, is a consequence of the unphysical nature of the barrier which forces the electronic density to vanish at a specific point thus causing the exchange charge to pile up at and about the jellium edge (see Fig. 1 of Ref. 7). In Fig. 1 we plot these slices in the step model for various positions of the electron outside the surface at $y=8, 20,$ and 50 . [The shape of the slice when the electron is inside the metal is the same as in the infinite barrier model and is given in Fig. 1(a) of Ref. 7.] A study of Fig. 1 shows that there is an order of magnitude decrease in the amplitude of the first peak as the electron is taken from $y=8$ to $y=50$. For the electron at $y=8$ and 20 [Figs. 1(a) and 1(b)], however, there is an evident decrease in amplitude of the succeeding peaks. But when the electron is at $y=50$ [Fig. 1(c)], the diminution of the amplitude of the successive peaks is negligible, and these essentially equivalent (through decreasing) amplitude oscillations continue for substantial distances into the metal. Furthermore, in comparison with the magnitude of the cross-section value (which is unity) at the position of the electron when it is inside the metal, there is a 2-order of magnitude diminution in the amplitude of the oscillations when the electron is at $y=50$. It is evident that the exchange charge which is symmetrical and localized about the electron when it is inside the metal [see Fig. 1(a) of Ref. 7] has now spread out in the crystal

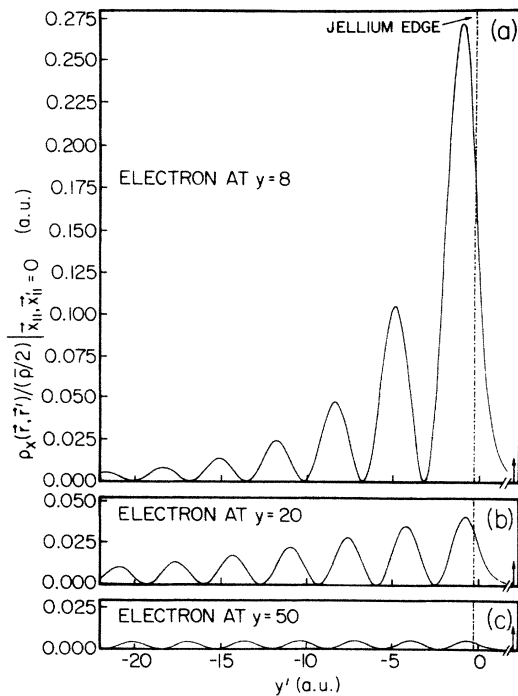


FIG. 1. Variation of the cross section $\rho_x(\mathbf{r}, \mathbf{r}') / (\rho/2) |_{x_{||}=x'_{||}=0}$ of the average exchange charge density $\rho_x(\mathbf{r}, \mathbf{r}')$ vs $y' = k_F x'$ in the step-potential model for different positions y of the electron in the vacuum. [See Eq. (6) of text.] The wave functions employed correspond to a barrier height parameter value of $\beta=0.8165$.

when the electron is far from the surface.

The cross sections discussed above are not adequate if we are to draw any conclusions regarding the amount of charge in a given region of space, or to determine the Slater potential⁸ due to the three-dimensional charge distribution. We therefore plot in Fig. 2 the planar-averaged exchange charge density given by Eq. (9) for the same positions of the electron as considered above. The planar-averaged charge, as discussed above, is the total charge in the plane at y' parallel to the surface, and consequently charge conservation requires that integration under these curves yield unity. We observe that the general trends for the planar averaged charge are the same as those for the cross section of the charge discussed previously (compare Fig. 1 and Fig. 2). Again note, that as the electron is pulled further out from the surface, the charge at the surface begins to diminish and the excess charge is pushed deeper into the metal: the amplitude of the first few oscillations diminish whereas those of the succeeding oscillations increase at their expense since charge conservation must be satisfied. Figure 2(c) shows that when the electron is at $y=50$, the amplitude of the oscillations though decreasing are essentially the same for large distances into the metal. As the electron is pulled out still further, the amplitude of these oscillations will decrease because the integral from minus to plus infinity must be unity. In the asymptotic limit, this charge will spread over the entire length of the semi-infinite crystal.

In order to study how the charge spreads asymptotically deep in the bulk, we derive in Appendix B the y' dependence of the planar-averaged exchange charge density. We show there that for *arbitrary* position y of the

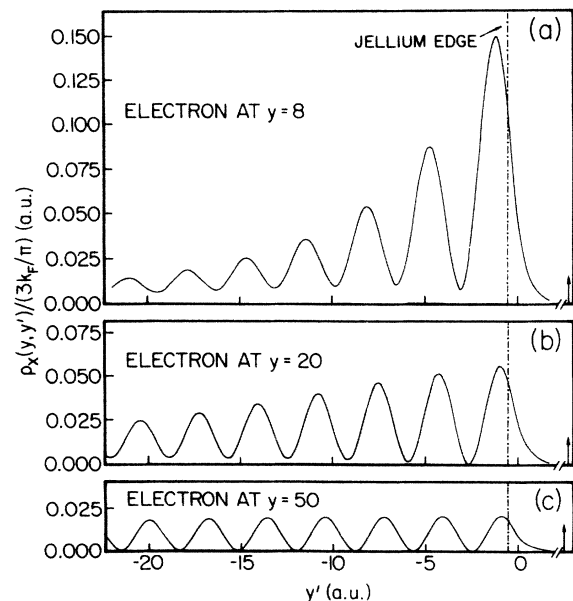


FIG. 2. Variation of the planar-averaged exchange charge density $\rho_x(y, y')$ vs $y' = k_F x'$ in the step-potential model for different positions y of the electron in the vacuum. [See Eqs. (8) and (9) of the text.] The barrier height parameter value assumed is $\beta=0.8165$.

electron, $\rho_x(y, y') \sim y'^{-2}$ for $y' \ll 0$. This derivation is independent of the model used to represent the potential at the surface. [However, the asymptotic dependence of the exchange charge density is most obviously evident from the infinite barrier model expression for $\rho_x(y, y')$ given in the Appendix of Ref. 7.] The implication here is that this will be the asymptotic dependence even in the case in which the surface potential is derived in a fully self-consistent manner.

That there is a charge at $y' = -\infty$ can be seen by considering the center of mass of the Fermi hole. It is evident that the integral

$$\langle y' \rangle = \int_{-\infty}^{\infty} y' \rho_x(y, y') dy' \sim \ln |y'|$$

is weakly divergent in the limit $y' \rightarrow -\infty$. If there were no charge at minus infinity, or equivalently if the extent of the exchange charge distribution was finite, the integral $\langle y' \rangle$ would converge. [Remember that the integral $\int_{-\infty}^{\infty} \rho_x(y, y') dy'$ does converge, and its value is unity. Also note that for the homogeneous electron gas, $\langle y' \rangle$ equals y .] Thus we see that there is a tail of the exchange charge density extending all the way up to minus infinity.

The derivation of the analytical behavior of the planar-averaged Fermi hole deep in the bulk also enables us to determine how rapidly the exchange charge spreads into the crystal. Let us consider an electron asymptotically far outside the surface at $y \gg 0$, so that $-y \ll 0$. Let us also assume that the dependence $\rho_x(y, y') \sim y'^{-2}$ is valid in the region $-\infty \leq y' \leq -y$. Consequently, the amount of charge in this region $\int_{-\infty}^{-y} \rho_x(y, y') dy' \sim y^{-1}$, and thus the amount of charge between $-y$ (inside the crystal) and $+\infty$ (outside in the vacuum region) must go as $(y-1)/y$. (Note that $[(y-1)/y] \rightarrow 1$ as $y \rightarrow \infty$ as it should because $\lim_{y \rightarrow \infty} \int_{-\infty}^{\infty} \rho_x(y, y') dy' = 1$.)

In Fig. 3 we plot the amount of charge in the region $-y \leq y' \leq \infty$ versus the electron position y outside the crystal. At $y=0$, there is very little charge outside as most of it is concentrated at and inside the surface. As the electron is removed further out, there is an initial increase in the value of the integral. This occurs because there is a pile-up of the exchange charge at the barrier—the charge is forced to remain within the metal. After reaching a maximum, the integral value decreases slowly as now the exchange charge is being pushed into the interior of the crystal beyond $-y$. The horizontal dashed line at unity represents the total exchange charge. Thus the value between the dashed line and the curve represents the amount of charge in the region $-\infty \leq y' \leq -y$. For example, for an electron at $y=4$ outside, 48% of the exchange charge lies in this region, whereas for $y=22$ there is 55% of the charge in the bulk. Even at $y=50$, there is 58% of the charge in the deep interior of the crystal. (Note that in the dimensionless variables used, $y=2\pi$ corresponds to a Fermi wavelength λ_F . The position $y=50$ could correspond to a distance of as much as 80 Å from the surface for a low-density metal such as Cs for which $\lambda_F \sim 10$ Å.) Thus from this model calculation we see that even for

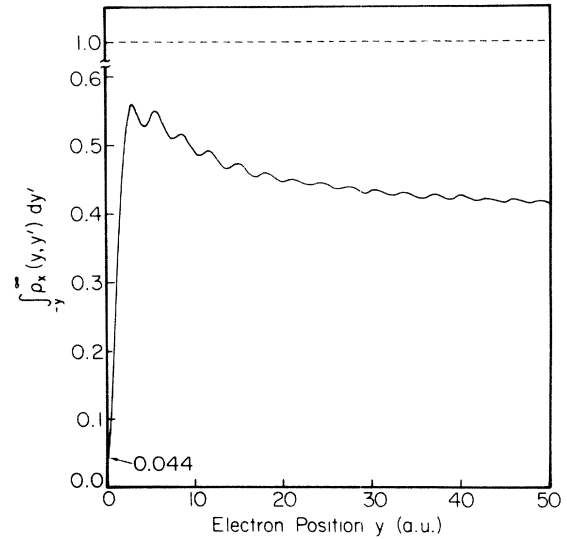


FIG. 3. Variation of the total charge between $-y$ and ∞ as given by the integral $\int_{-y}^{\infty} \rho_x(y, y') dy'$ vs the electron position $y = k_F x$ in the step-potential model. The barrier height parameter value assumed is $\beta = 0.8165$.

asymptotic positions of the electron outside the metal, there is a substantial fraction of the exchange charge that lies in the deep interior of the metal.

In Fig. 4 we plot the planar charge distribution of Eq. (4) for the same electron positions outside the metal as those of Figs. 1 and 2. In Fig. 4(a) the curves are drawn for the positions y' corresponding to the first two peaks of Fig. 1(a), those of Fig. 4(b) correspond to the first and third peaks of Fig. 1(b), and those of Fig. 4(c) to the first and sixteenth peaks of Fig. 1(c). Note [see Fig. 4(a)] that when the electron is near the surface the charge distribution taken radially from the axis of electron removal falls off rapidly. As the electron is removed further outside the metal [Figs. 4(b) and 4(c)] the planar charge spreads out more radially and its fall off rate diminishes. Thus in the asymptotic limit the charge also spreads out radially over the entire crystal.

The results of Figs. 1, 2, and 4 thus prove that as an electron is removed from a metal, its exchange charge distribution takes the shape of equally spaced disks. These disks have substantial charge at and near the surface when the electron is close to it. In the asymptotic limit as the electron is removed to infinity outside, these disks of charge distribute themselves not only over the entire length of the crystal but also radially over its entire width. Thus in this limit the exchange charge is not localized near the surface of the metal but rather spread over its entire volume.

The obvious next question of interest is what is the corresponding behavior of the Slater potential to which this unit charge gives rise? The answer to this question and other related work on the potential (see our concluding remarks) is in progress and as such is relegated to a future publication.¹⁶ However, we do know that for a point charge outside a metal surface, the classical image charge leads to an image potential. In order to get some

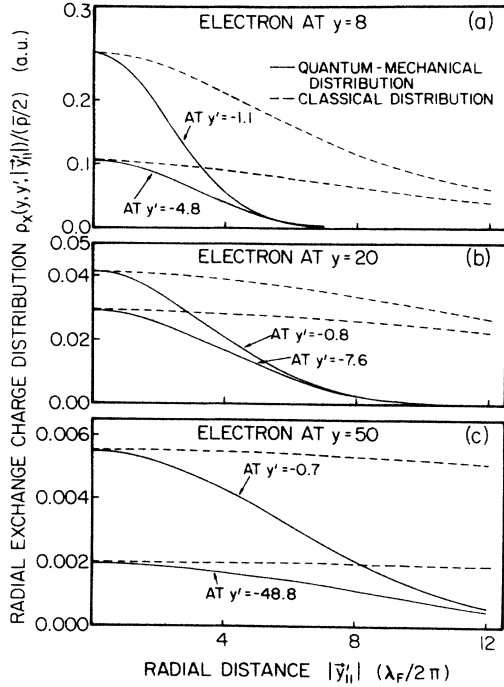


FIG. 4. Variation of the radial distribution of the exchange charge density in planes at y' parallel to the surface vs the distance from the axis along which the electron is being removed. The graphs are drawn for the step-potential model for different positions y of the electron outside the surface. The value of the barrier height parameter is $\beta=0.8165$. The solid lines correspond to the quantum-mechanical charge distribution, whereas the dashed lines represent the classical distribution of charge. [See Eqs. (4) and (14) of text.]

insights into the behavior of the Slater potential,⁸ let us examine how different the quantum-mechanical and classical distributions of charge are. The classical image charge, which is spread over the entire surface, has zero width in the direction perpendicular to it. For an electron at y outside the surface, the classical image charge density at $|y'_{||}|$ in the plane of the surface is given by the expression

$$\sigma(|y'_{||}|) = \frac{\sigma_0 y^3}{(y^2 + |y'_{||}|^2)^{3/2}}, \quad (13)$$

where σ_0 is the surface charge density at $|y'_{||}|=0$, the axis of electron removal. The quantum-mechanical distribution of charge, on the other hand, is three dimensional, and extends into the metal. Consequently, for purposes of comparison we assume the classical charge distribution to have the quantum-mechanical dependence in the direction perpendicular to the surface. In the planes parallel to the surface we assume the same analytical form as derived from classical electrostatics. Thus, in Fig. 4 we also plot the quantity

$$\rho_x^{\text{classical}}(y, y', |y'_{||}|) = \frac{\rho_x(y, y', |y'_{||}|=0)(y-y')^3}{[(y-y')^2 + |y'_{||}|^2]^{3/2}}. \quad (14)$$

It is clear from the figure that the classical charge distri-

bution bears little resemblance to the quantum-mechanical distribution: it is always an overestimate. Thus in order to ensure the satisfaction of the charge conservation sum rule of Eq. (3), the classical distribution would have to be cut off at some point in the plane. As a consequence of the differences between the shapes of the two charge distributions (and the fact that the classical distribution has a cutoff), one would expect that the corresponding potentials would also be different.

As indicated earlier, the step-potential model is adequate only for a qualitative description of a metal surface: the magnitudes of the properties of interest can be significantly different from those of any more accurate representation of the effective potential at a surface. Consequently, in order to obtain a more realistic representation of the average exchange charge density as well as to study how a softer potential affects the three-dimensional distribution of the hole throughout the crystal, we repeat our calculations for the physically more accurate linear-potential model^{14,17} of a surface. (This was the model considered by Sahni and Bohnen.^{6,7})

The effective potential in this case is $V_{\text{eff}}=Fx\Theta(x)$, and the wave functions $\phi_k(x)$ in the direction perpendicular to the surface are

$$\begin{aligned} \phi_k(x) = & \sin[kx + \delta(k)]\Theta(-x) \\ & + \sin\delta(k) \frac{\text{Ai}(-\xi)}{\text{Ai}(-\xi_0)} \Theta(x), \end{aligned} \quad (15)$$

with $\delta(k) = \cot^{-1}[\text{Ai}'(-\xi_0)/(\xi_0)^{1/2}\text{Ai}(-\xi_0)]$, and where $\text{Ai}(\xi)$ and $\text{Ai}'(\xi)$ are the Airy functions and their derivatives, respectively; $\xi = x(k_F^2/x_F)^{1/3} - \xi_0$; $\xi_0 = (k_F x_F)^{2/3} k^2 / k_F^2$, and $F = (k_F^2/2)/x_F$.

As in the case of the step model, all the surface properties for this model potential can also be written¹⁴ in terms of functions of the slope or field strength parameter $y_F = k_F x_F$. By varying y_F , one can change continuously the electronic density profile at the surface from very rapidly varying to very slowly varying. For our calculations we have chosen $y_F=3$, a typical¹⁸ metallic density profile.

In Figs. 5 and 6 we graph, respectively, the cross section of the Fermi hole and its planar average as obtained for the wave functions of Eq. (15). A comparison of these graphs with those of Figs. 1 and 2 of the step model clearly indicates similar trends in the behavior of the various charge distributions. The magnitudes of the densities are more or less the same for electron positions close to the surface [compare panels (a) of the appropriate graphs]. However, as the electron is pulled further out the decrease of charge near the surface is not quite as dramatic as in step-model case. For an electron at $y=20$, the amplitude of the first peak of the cross section in the linear-potential case is four times as large [compare Figs. 1(b) and 4(b)], whereas that for the planar-averaged density is twice as large [compare Figs. 2(b) and 5(b)]. Thus for the same electron position, there is clearly more charge near the surface in the softer more realistic linear-potential model than there is in the step model. [Panels (c) of Figs. 5 and 6 have been plotted for currently maximum allowed electron positions of

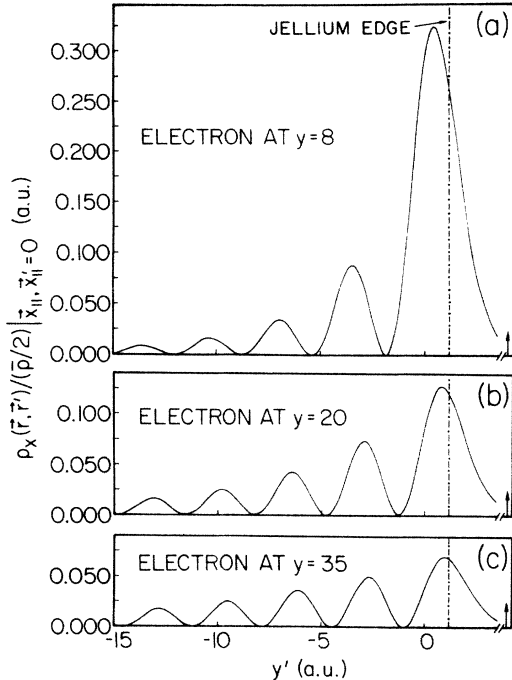


FIG. 5. The figure caption is the same as that of Fig. 1 except that these curves have been drawn for the linear potential model wave functions corresponding to a value of $y_F=3$ for the slope parameter.

$y=35$ and 30 , respectively, since it was not possible to go beyond these points due to numerical underflow.] As a consequence, the spreading of charge into the interior of the crystal is not as rapid. This is evident in a comparison of Figs. 3 and 7 for the integral $\int_{-\infty}^y \rho_x(y, y') dy'$, the latter figure corresponding to the

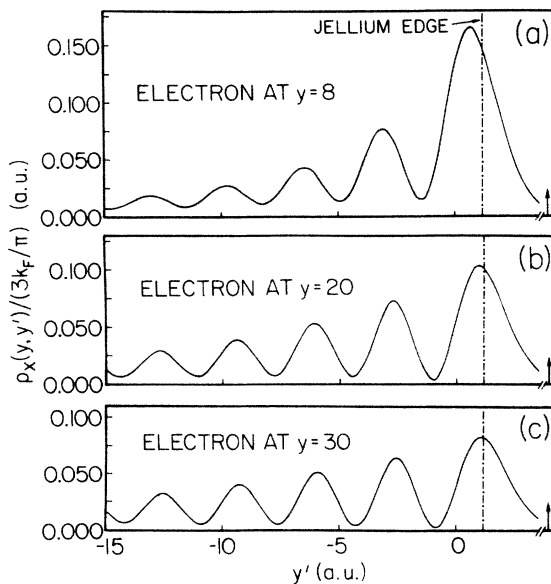


FIG. 6. The figure caption is the same as that of Fig. 2 except that these curves have been drawn for the linear potential model wave function for a value of $y_F=3$ for the slope parameter.

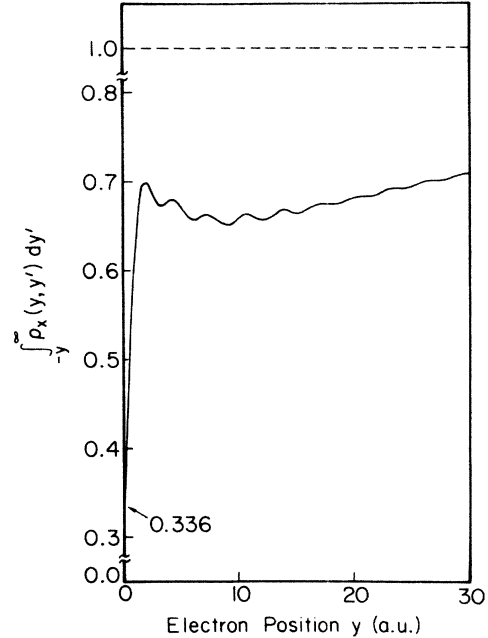


FIG. 7. The figure caption is the same as that of Fig. 3 except that this curve has been drawn for the linear potential model wave functions corresponding to a value of $y_F=3$ for the slope parameter.

linear-potential model. For a specific electron position, the magnitude of the graph in Fig. 7 is always greater than that of Fig. 3. This means that the charge in the region $-\infty \leq y' \leq -y$ is less and that its decrease at the surface as the electron is pulled further out is not as rapid as in the step model. (For electron positions at $y=4$ and 22 , the charge in the region $-\infty \leq y' \leq -y$ is 32% and 31% , respectively. The corresponding values for the step model are 48% and 55% , respectively.) Figure 8 shows the charge distribution in the planes parallel to the surface. Observe that here the charge diminishes in the direction perpendicular to the axis of electron removal more rapidly than in the step case (Fig. 4). This again is a consequence of the fact that the linear potential is softer than the step potential, thus allowing more electrons within the surface region to interact with the electron outside. Finally, since the fall off of the more realistic quantum-mechanical charge in the planes parallel to the surface is more rapid than in the step model, the differences in this case between the true and classical distributions of charge is even greater (compare Figs. 4 and 8). As a consequence one would expect the resulting differences in the potentials due to the charge distribution to also be more significant.

III. CONCLUDING REMARKS

In conclusion, we have extended the work of Sahni and Bohnen to more emphatically demonstrate that as an electron is removed from within a metal to infinity outside, its average exchange charge density is not localized to the surface region but rather spreads out throughout the entire crystal. That there is always

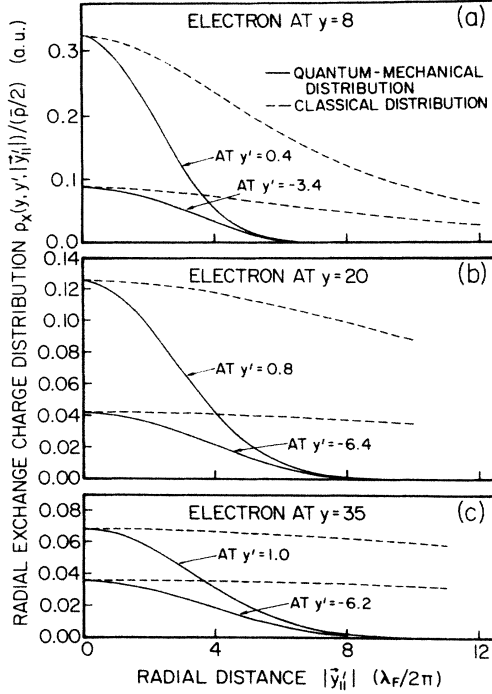


FIG. 8. The figure caption is the same as that of Fig. 4 except that these curves have been drawn for the linear potential model wave functions corresponding to a value of $y_F = 3$ for the slope parameter.

charge at minus infinity, irrespective of the electron position at or outside the metal, has been shown analytically. Thus when the electron is asymptotically far from the surface, its Fermi hole does not constitute part of the image charge at the surface. The physics of why this occurs is clear. When the electron is far outside, only those electrons with high energy in the metal can interact with it. By this we mean that it is only those electrons within a small range of energies below the Fermi level whose wave functions can reach and overlap the electron. In the asymptotic limit it is only the Fermi level electrons with momentum perpendicular to the surface whose wave functions overlap the asymptotic electron. Thus it is evident from Eq. (1) that for an asymptotic electron, its Fermi hole goes as¹⁹ $|\Psi_{k_F}(\mathbf{r})|^2$, which is a density spread throughout the crystal.

In this paper we have studied the behavior of the *average* exchange charge density at surfaces. Work towards the determination of the potential to which this *unit* charge gives rise, the Slater potential, is in progress and will be reported elsewhere.¹⁶ This is an orbital indepen-

dent potential and is the same for each electron. An analytical expression for this potential for wave functions generated by the infinite barrier model has been derived.^{1,20} Thus what is of particular interest is its asymptotic behavior because this is a result that cannot be obtained within the infinite barrier model approximation. Furthermore, the result would be fascinating in its own right since in the asymptotic region the potential is due to a rather interesting distribution of charge viz. an infinite number of parallel sheets of total charge unity extending throughout the crystal. This distribution is also significantly different from the classical distribution which is a single sheet of zero thickness charge at the surface.

Now, although the average exchange charge density is the property required for the determination of the exchange energy, it is not this hole which appears in the Hartree-Fock equations. The Fermi hole of Hartree-Fock theory is *orbital dependent* and is defined as

$$\rho_{x,k}(\mathbf{r}, \mathbf{r}') = \sum_{k'} \frac{\Psi_{k'}^*(\mathbf{r}') \Psi_{k'}(\mathbf{r}) \Psi_{k'}(\mathbf{r}')}{\Psi_{k'}(\mathbf{r})} \quad (16)$$

Due to the orthonormality of the wave functions, it too satisfies the charge conservation sum rule. We are also presently investigating¹⁶ the behavior of the orbital-dependent Fermi hole as well as the corresponding orbital-dependent exchange potentials at surfaces. It is, however, explicitly evident that on applying the same reasoning as in the first paragraph of these remarks to Eq. (16), the orbital-dependent Fermi hole too must have the same asymptotic behavior as observed in the present work. Thus we expect the asymptotic behavior of the higher energy orbital-dependent potentials to be the same as those of the Slater potential.

Note added in proof. We have recently²² determined the asymptotic structure of the Slater potential to be image-potential-line with a coefficient of $3/2\pi$, approximately twice as large as the image-potential coefficient of $\frac{1}{4}$.

ACKNOWLEDGMENT

This work was supported in part by the Research Foundation of the City University of New York, Professional Staff Congress—Board of Higher Education.

APPENDIX A: EXCHANGE CHARGE DENSITY AND ITS PLANAR AVERAGE

In this appendix we derive Eq. (4) for the average exchange charge density and prove the equivalence of Eqs. (8) and (9) for the planar-averaged density. On substituting Eq. (2) into Eq. (1) of the text, the expression for the average exchange charge density is

$$\rho_x(\mathbf{r}, \mathbf{r}') = \frac{1}{\rho(\mathbf{r})/2} \frac{1}{A^2} \left[\frac{2}{L} \right]^2 \sum_{k, k_{\parallel}} \sum_{k', k'_{\parallel}} \Theta(k_F^2 - k^2 - k_{\parallel}^2) \Theta(k_F^2 - k'^2 - k'_{\parallel}^2) e^{i(k_{\parallel} - k'_{\parallel}) \cdot (x'_{\parallel} - x_{\parallel})} \phi_k^*(x) \phi_{k'}^*(x') \phi_k(x') \phi_{k'}(x) \quad (A1)$$

$$= \frac{1}{2\pi^6 \rho(\mathbf{r})} \int_0^{k_F} dk \int_0^{k_F} dk' \phi_k^*(x) \phi_{k'}^*(x') \phi_k(x') \phi_{k'}(x) \left[\int_0^{(k_F^2 - k^2)^{1/2}} k_{\parallel} dk_{\parallel} \int_0^{2\pi} d\theta e^{ik_{\parallel} x'_{\parallel} \cos\theta} \right] \\ \times \left[\int_0^{(k_F^2 - k'^2)^{1/2}} k'_{\parallel} dk'_{\parallel} \int_0^{2\pi} d\theta' e^{ik'_{\parallel} x'_{\parallel} \cos\theta'} \right]. \quad (A2)$$

Now²¹ the integral

$$\begin{aligned} \int_0^{(k_F^2 - k^2)^{1/2}} k_{\parallel} dk_{\parallel} \int_0^{2\pi} d\theta e^{ik_{\parallel} x'_{\parallel} \cos\theta} &= 2\pi \int_0^{(k_F^2 - k^2)^{1/2}} k_{\parallel} dk_{\parallel} J_0(k_{\parallel} x'_{\parallel}) \\ &= 2\pi \frac{(k_F^2 - k^2)^{1/2}}{x'_{\parallel}} J_1[(k_F^2 - k^2)^{1/2} x'_{\parallel}] , \end{aligned} \quad (\text{A3})$$

so that Eq. (A2) becomes

$$\rho_x(\mathbf{r}, \mathbf{r}') = \frac{2}{\pi^4 \rho(\mathbf{r})} \left| \int_0^{k_F} dk \phi_k^*(x) \phi_k(x') \frac{(k_F^2 - k^2)^{1/2}}{x'_{\parallel}} J_1[(k_F^2 - k^2)^{1/2} x'_{\parallel}] \right|^2 . \quad (\text{A4})$$

Here $J_0(x)$ and $J_1(x)$ are the zeroth- and first-order Bessel functions, respectively. Changing to the dimensionless variables $q = k/k_F$, $q' = k'/k_F$ and $y = k_F x$, $y'_{\parallel} = k_F x'_{\parallel}$, one gets

$$\frac{\rho_x(y, y'; y'_{\parallel})}{(\bar{\rho}/2)} = \frac{36}{\rho_n(y)} \left| \int_0^1 dq \phi_q^*(y) \phi_q(y') \frac{(1-q^2)^{1/2}}{|y'_{\parallel}|} J_1[(1-q^2)^{1/2} |y'_{\parallel}|] \right|^2 , \quad (\text{A5})$$

which is Eq. (4) of the text. This is the average exchange charge density at (y', y'_{\parallel}) for an electron at y . The planar-averaged exchange charge is therefore

$$\begin{aligned} \rho_x(y, y') &= \int d\mathbf{x}'_{\parallel} \rho_x(\mathbf{r}, \mathbf{r}') \\ &= \frac{1}{k_F^2} \int dy'_{\parallel} \rho_x(y, y'; y'_{\parallel}) . \end{aligned} \quad (\text{A6})$$

Substituting the expression for $\rho_x(y, y'; y'_{\parallel})$ from Eq. (A5) into Eq. (A6) one can write

$$\begin{aligned} \rho_x(y, y') &= \frac{36\pi\bar{\rho}}{\rho_n(y)} \int_0^{\infty} \frac{d|y'_{\parallel}|}{|y'_{\parallel}|} \int_0^1 dq \int_0^1 dq' \phi_q^*(y) \phi_q(y') \phi_{q'}(y) \phi_{q'}^*(y') (1-q^2)^{1/2} (1-q'^2)^{1/2} \\ &\quad \times J_1[(1-q'^2)^{1/2} |y'_{\parallel}|] J_1[(1-q^2)^{1/2} |y'_{\parallel}|] . \end{aligned} \quad (\text{A7})$$

Now²¹ the integral

$$\int_0^{\infty} \frac{dR}{R} J_1[(1-q^2)^{1/2} R] J_1[(1-q'^2)^{1/2} R] = \begin{cases} \frac{(1-q'^2)^{1/2}}{2(1-q^2)^{1/2}} F\left[1, 0; 2; \frac{(1-q'^2)}{(1-q^2)}\right] & \text{for } q < q' , \\ \frac{(1-q^2)^{1/2}}{2(1-q'^2)^{1/2}} F\left[1, 0; 2; \frac{(1-q^2)}{(1-q'^2)}\right] & \text{for } q > q' , \end{cases} \quad (\text{A8})$$

where $F(\alpha, \beta; \gamma; z)$ is the hypergeometric function, and $F(\alpha, \beta; \gamma; z) = 1$ for either $\alpha = 0$ or $\beta = 0$. Therefore we may write Eq. (A7) as

$$\begin{aligned} \rho_x(y, y') &= \frac{1}{2} \frac{36\pi\bar{\rho}}{k_F^2 \rho_n(y)} \left[\int_0^1 dq \int_0^q dq' \phi_q^*(y) \phi_q(y') \phi_{q'}(y) \phi_{q'}^*(y') (1-q^2) \right. \\ &\quad \left. + \int_0^1 dq \int_q^1 dq' \phi_q^*(y) \phi_q(y') \phi_{q'}(y) \phi_{q'}^*(y') (1-q'^2) \right] . \end{aligned} \quad (\text{A9})$$

Since both the integrals are over the triangle (0,0), (1,0), and (1,1) in the (q', q) plane, we can write the second integral of Eq. (A9) as

$$\int_0^1 dq' \int_0^{q'} dq \phi_q^*(y) \phi_q(y') \phi_{q'}(y) \phi_{q'}^*(y') (1-q'^2) . \quad (\text{A10})$$

Interchanging q and q' in Eq. (A10) one gets the integral

$$\int_0^1 dq \int_0^q dq' \phi_{q'}^*(y) \phi_{q'}(y') \phi_q(y) \phi_q^*(y') (1-q^2) , \quad (\text{A11})$$

which is the complex conjugate of the first integral. The planar-averaged charge therefore is

$$\rho_x(y, y') = \frac{12k_F}{\pi\rho_n(y)} \text{Re} \left[\int_0^1 dq (1-q^2) \phi_q^*(y) \phi_q(y') \int_0^q dq' \phi_{q'}^*(y') \phi_{q'}(y) \right] , \quad (\text{A12})$$

which is the same as Eq. (9) of the text.

APPENDIX B: ASYMPTOTIC BEHAVIOR OF THE PLANAR-AVERAGED EXCHANGE CHARGE DENSITY

In this appendix we derive the y' dependence of the planar-averaged exchange charge density deep in the bulk (i.e., for $y' \ll 0$) independent of the position y of the electron. For real ϕ 's [see Eq. (2)] the expression for the planar-averaged exchange charge density given by Eq. (9) may be rewritten as

$$\rho_x(y, y') = \frac{36k_F}{\pi\rho_n(y)} \int_0^1 dq (1-q^2) \phi_q(y') \phi_q(y) \int_0^q dq' \phi_{q'}(y') \phi_{q'}(y). \quad (\text{B1})$$

For $y' \ll 0$, $\phi_{q'}(y')$ can be approximated as $\sin(q'y')$ by ignoring the phase shift $\delta(q')$ so that

$$\begin{aligned} \int_0^q dq' \phi_{q'}(y') \phi_{q'}(y) &= \int_0^q dq' \sin(q'y') \phi_{q'}(y) \\ &= -\frac{\cos(qy')}{y'} \phi_q(y) + \frac{1}{y'^2} \sin(qy') \frac{d}{dq} \phi_q(y) - \frac{1}{y'^2} \int_0^q dq' \sin(q'y') \frac{d^2 \phi_{q'}(y)}{dq'^2}. \end{aligned} \quad (\text{B2})$$

Now for wave functions which are either exponential (as they are in the classically forbidden region) or oscillatory (as in the metal),

$$\frac{d^2 \phi_{q'}(y)}{dq'^2} \sim y^2 \phi_{q'}(y). \quad (\text{B3})$$

[In the case of the linear-potential model $d^2 \phi_{q'}(y)/dq'^2 \sim y \phi_{q'}(y)$]. Substituting Eq. (B3) into Eq. (B2) we obtain

$$\int_0^q dq' \phi_{q'}(y') \phi_{q'}(y) \sim -\frac{\cos(qy')}{y'} \phi_q(y) + \frac{1}{y'^2} \sin(qy') \frac{d}{dq} \phi_q(y) - \left[\frac{y}{y'} \right]^2 \int_0^q dq' \sin(q'y') \phi_{q'}(y). \quad (\text{B4})$$

The last integral in Eq. (B4) is the same as the integral we started with, so that the last term is of $O(y'^{-3})$ and therefore may be ignored. Thus one may write

$$\begin{aligned} \rho_x(y, y' \rightarrow \infty) &\sim \frac{36k_F}{\pi\rho_n(y)} \int_0^1 dq (1-q^2) \sin(qy') \phi_q(y) \left[-\frac{\cos(qy')}{y'} \phi_q(y) + \frac{\sin(qy')}{y'^2} \frac{d}{dq} \phi_q(y) \right] \\ &= \frac{1}{y'^2} \left[\frac{9k_F}{\pi\rho_n(y)} \int_0^1 dq (1-q^2) \frac{d}{dq} [\phi_q^2(y)] \right] - \frac{1}{y'} \left[\frac{18k_F}{\pi\rho_n(y)} \int_0^1 dq (1-q^2) \sin(2qy') \phi_q^2(y) \right] \\ &\quad - \frac{1}{y'^2} \left[\frac{9k_F}{\pi\rho_n(y)} \int_0^1 dq (1-q^2) \cos(2qy') \frac{d}{dq} \phi_q^2(y) \right]. \end{aligned} \quad (\text{B5})$$

The integrals of the second and third terms are rapidly oscillating functions for $y' \rightarrow -\infty$, so that retaining the leading term of Eq. (B5) we have

$$\begin{aligned} \rho_x(y, y' \rightarrow -\infty) &\sim \frac{1}{y'^2} \left[\frac{9k_F}{\pi\rho_n(y)} \int_0^1 dq (1-q^2) \frac{d}{dq} \phi_q^2(y) \right] \\ &= \frac{1}{y'^2} \left[\frac{18k_F}{\pi\rho_n(y)} \int_0^1 dq q \phi_q^2(y) \right]. \end{aligned} \quad (\text{B6})$$

Thus the leading term in $\rho_x(y, y')$ as $y' \rightarrow -\infty$ goes as $(y')^{-2}$.

¹H. J. Juretschke, Phys. Rev. **92**, 1140 (1953). In this work an approximate expression for the cross section through the Fermi hole in the direction perpendicular to the surface was derived which "shows that the single exchange hole is replaced by a series of disklike charge distributions of equal magnitude spaced at intervals of π/k_F up to a distance equal to the distance of the electron from the surface." Thus it was concluded that "the exchange hole remains in the surface" region.

²J. Bardeen, Surf. Sci. **2**, 381 (1964).

³D. S. Boudreaux and H. J. Juretschke, in *Structure and Properties of Metal Surfaces* (Maruzen, Tokyo, 1973). These authors state that, "as the electron approaches the surface its exchange hole remained behind in the region of high charge

density, eventually flattening out to a thin planar charge defect excluding in total a charge of $-|e|$ when the electron is infinitely far away."

⁴J. E. Inglesfield and I. D. Moore, Solid State Commun. **26**, 867 (1978).

⁵N. D. Lang, in *Theory of the Inhomogeneous Electron Gas*, edited by S. Lundquist and N. H. March (Plenum, New York, 1983).

⁶V. Sahni and K.-P. Bohnen, Phys. Rev. B **29**, 1045 (1984).

⁷V. Sahni and K.-P. Bohnen, Phys. Rev. B **31**, 7651 (1985).

⁸J. C. Slater, Phys. Rev. **81**, 385 (1951).

⁹Atomic units are used: $|e| = \hbar = m = 1$.

¹⁰J. Bardeen, Phys. Rev. **49**, 653 (1936).

¹¹V. Sahni, J. B. Krieger, and J. Gruenebaum, Phys. Rev. B **12**,

- 3503 (1975).
- ¹²V. Sahni and J. Gruenebaum, *Phys. Rev. B* **15**, 1929 (1977).
- ¹³N. D. Lang and W. Kohn, *Phys. Rev. B* **1**, 4555 (1970); **3**, 1215 (1971).
- ¹⁴V. Sahni, J. B. Krieger, and J. Gruenebaum, *Phys. Rev. B* **15**, 1941 (1977); V. Sahni and J. Gruenebaum, *Solid State Commun.* **21**, 463 (1977).
- ¹⁵V. Sahni, C. Q. Ma, and J. S. Flamholz, *Phys. Rev. B* **18**, 3931 (1978).
- ¹⁶M. K. Harbola and V. Sahni (unpublished).
- ¹⁷J. P. Perdew and V. Sahni, *Solid State Commun.* **30**, 87 (1979).
- ¹⁸V. Sahni, J. P. Perdew, and J. Gruenebaum, *Phys. Rev. B* **23**, 6512 (1981).
- ¹⁹M. Levy, J. P. Perdew, and V. Sahni, *Phys. Rev. B* **30**, 2745 (1984).
- ²⁰L. Miglio, M. P. Tosi, and N. H. March, *Surf. Sci.* **111**, 119 (1981) have rederived the expression for the Slater potential in the infinite barrier model, as given in Ref. 1. Also see review article by N. H. March in Ref. 5.
- ²¹*Table of Integrals, Series, and Products*, edited by I. S. Gradshteyn and I. M. Ryzhik (Academic, New York, 1980).
- ²²M. K. Harbola and V. Sahni, *Phys. Rev. B* **36**, 5024 (1987).